Energy-loss rate of a two-dimensional electron gas measured using a mesoscopic thermometer

Y. Y. Proskuryakov, J. T. Nicholls, and D. I. Hadji-Ristic
Department of Physics, Royal Holloway, University of London, Egham, Surrey TW20 0EX, United Kingdom

A. Kristensen* and C. B. Sørensen
Ørsted Laboratory, Niels Bohr Institute, Universitetsparken 5, DK-2100 Copenhagen, Denmark
(Received 14 August 2006; revised manuscript received 3 November 2006; published 5 January 2007)

Using a simple setup, the linear thermopower is measured in etched one-dimensional (1D) constrictions with large subband energy spacings, allowing the temperature of the two-dimensional electron gas on one side of the constriction to be determined as a function of the applied heating power. As tested by the Cutler-Mott relation, the 1D constriction acts as a reliable electron thermometer for lattice temperatures in the range T_L =4.2–13 K. The power dissipated per electron, measured as a function of electron temperature, reveals that at T_L=4.2 K the acoustic phonon scattering is dominated by T^5 behavior due to an unscreened deformation potential. At higher lattice temperatures the scattering can be described by an interpolation between the Grüneisen-Bloch and equipartition regimes.

DOI: 10.1103/PhysRevB.75.045308 PACS number(s): 73.23.Ad, 72.20.Pa, 63.20.Kr

I. INTRODUCTION

Tunable constrictions in high-mobility two-dimensional electron gases (2DEGs) have allowed the study of one-dimensional (1D) ballistic transport. Typically a voltage V_g applied to a surface gate controls the number of transverse modes transmitted through the constriction, and in wires shorter than 1 μm the differential conductance characteristics $G(V_g)=dI/dV$ exhibit[1,2] plateaus quantized at integer multiples of $2e^2/h$. A 1D constriction can also act as a calibrated thermometer, measuring the electron temperature (T_e) in a 2DEG on one side of the constriction.[3,4] Such a thermometer has been used to measure[5] the quantum thermal conductance of electrons passing through a 1D constriction.

When 2D electrons are heated to a temperature T_e above the lattice temperature T_L, they can lose their energy to acoustic phonons. At high temperatures in the equipartition regime (20–30 K) the phonons can be easily emitted, but at low temperatures (<4.2 K) there are phase restrictions on emission. The crossover temperature between these two regimes is the Grüneisen-Bloch (GB) temperature, which is defined as $T_{GB}=2\hbar s_t k_F/k_B$, where s_t is the transverse sound velocity and k_F is the Fermi wave vector. For a typical high-mobility 2DEG of carrier density $(1-2)\times 10^{11}$ cm^{-2}, the transition temperature is[6] $T_{GB}\approx 5-8$ K. In the Grüneisen-Bloch regime $T\ll T_{GB}$, the function form of the electron-phonon energy-loss rate is expected to be T^n, where $n=7$ for a screened deformation potential (DP) and $n=5$ for a screened piezoelectric (PZ) mechanism. The unscreened DP and PZ mechanisms occur with $n=5$ and 3, respectively. In the equipartition regime, $T\gg T_{GB}$, the energy-loss rate is proportional to T. In an earlier study[4] using split-gate constrictions measurements for $T_e<3$ K showed clear T^5 behavior, and the dominant scattering mechanism was found to be acoustic phonon scattering via a screened piezoelectric potential.

In this paper we investigate the thermal properties of the 2DEG by measuring the thermopower of 1D devices, where the constriction is formed by wet etching of the 2DEG mesa, which creates hard potential walls with large 1D subband energy spacings.[7] We use these etched structures for thermometry of the 2DEG at high lattice and electron temperatures T_e, $T_L\geq 4.2$ K, where the theoretical description of the GB regime with acoustic phonon scattering is expected to break down. Due to thermal smearing of the low-field oscillations, reliable thermometry of 2D electrons from the temperature dependence of the Shubnikov–de Haas oscillations is difficult for lattice temperatures $T_L>4.2$ K; so thermometry using constrictions with large 1D subband spacings is attractive. Studies of the mobility as a function of temperature to find the electron-phonon contribution are complicated, because at low temperatures impurity scattering makes an appreciable contribution to the mobility.[6] 1D thermometry in the ballistic regime bypasses any difficulties caused by impurity scattering.

II. SAMPLES AND MEASUREMENT TECHNIQUE

The scanning electron micrograph (SEM) image in Fig. 1(a) shows one of the three similar devices, consisting of a Hall bar with six Ohmic contacts on the 2DEG. Etching of the mesa creates a 1D constriction in the center of the Hall bar [see close-up SEM image in Fig. 1(b)] and by application of a voltage V_g to a macroscopic gate above this constriction the number of conducting 1D subbands can be varied. In contrast to conventional split-gate devices, V_g needs to be positive to make the 1D channel conducting.[7]

The electron thermometry used in this paper is based on a measurement of the linear thermopower, as described by Appleyard *et al.*,[4] except that here there is no second (reference) constriction to eliminate spurious voltages on the hot side of the device. We will demonstrate in Sec. III (see Figs. 1 and 2) that the reference is not necessary and that using just one etched 1D constriction allows stable and reproducible electron thermometry. Measurements were performed on three etched samples I, II, and III, with energy spacings ($\hbar\omega_y$) between the first and second 1D subbands of 14, 10, and 6 meV, respectively. Samples I and II were fabricated from

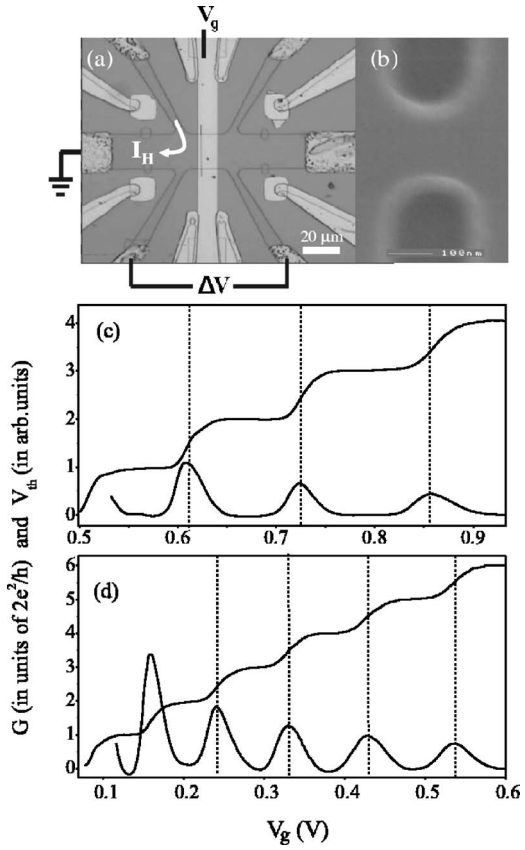

FIG. 1. (a) Scanning electron micrograph of a typical device showing the six Ohmic contacts on the Hall bar. A current I_H heats electrons on the left side of the sample, and a thermovoltage ΔV is measured across the 1D constriction. The power dissipated by the 2DEG on the left side of the sample is presented in later figures. (b) SEM close-up of the etched constriction, which is situated below the central gate. (c) Conductance $G(V_g)$ and thermovoltage characteristics of sample I at $T=4.2$ K, with $V_{th}(V_g)$ measured using a heating current of $I_H=1$ μA. (d) Similar measurements for sample III.

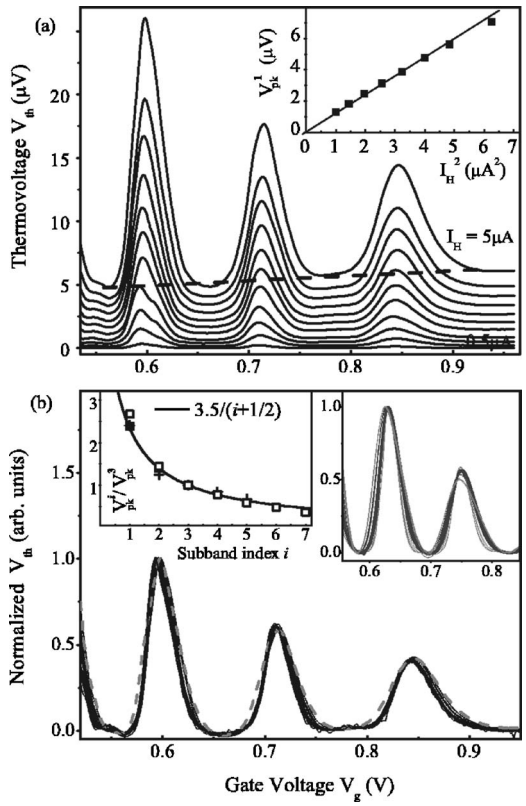

FIG. 2. (a) Thermovoltage measured at $T_L=4.2$ K at heating currents $I_H=0.5$, 1, 1.4, 1.8, 2.2, 2.5, 2.8, 3.2, 3.6, 4, and 5 μA. The dashed line shows the parasitic linear contribution at $I_H=5$ μA. Inset: the magnitude of the first thermovoltage peak plotted as a function of I_H^2. (b) Normalized thermovoltage traces measured at $T_L=4.2$ K for 17 values of heating current $I_H=0.5-6$ μA. The dashed gray line shows thermal broadening at $I_H=7$ μA. Left inset: the normalized peak heights V_{pk}^i/V_{pk}^3 for samples I (■), II (+), and III (□). Right inset: similar data to the main figure in (b), but measured at $T_L=4.2$, 6.9, 10, and 13 K.

one wafer, and sample III was fabricated from a similar wafer. In both cases the 2DEG is formed at a $GaAs/Al_xGa_{1-x}As$ heterojunction and has a mobility of 8×10^5 cm^2/V s and an electron density $n_e=2\times10^{11}$ cm^{-2}. The subband spacings in the etched samples are much greater than in conventional split-gate devices ($\sim1-3$ meV), and the high energy scale allows measurements of the linear thermopower S for lattice temperatures $T_L=4.2-13$ K.

Measurements were performed using the setup shown in Fig. 1(a), where a current I_H of frequency $f_1=18$ Hz is applied between two Ohmic contacts on the left side of the constriction, heating the electrons to a temperature T_e. Due to the temperature difference $\Delta T=T_e-T_L$, a thermoelectric voltage ΔV induced across the 1D constriction is measured at a frequency $2f_1$ between the third contact on the heated side, and one of the free contacts on the cold side. The measured ΔV is usually negative, and for convenience we present thermovoltage results as $V_{th}=-\Delta V$. An ac current of 10 nA at a frequency $f_2=230$ Hz was applied to one of the Ohmic contacts on the cold side. The current flows through the constriction into the same earth that sinks the heating current, and the resulting voltage drop allows the resistance $R(V_g)$ of the 1D constriction to be measured simultaneously with the thermovoltage $\Delta V(V_g)$. The resistance is inverted to obtain the conductance characteristics $G(V_g)$.

III. EXPERIMENTAL RESULTS AND DISCUSSION

Compared to previous studies[3,4] there is no second constriction in the thermopower setup to act as the reference. Consequently there is a small negative contribution to the $V_{th}(V_g)$ traces that depends on I_H and has a linear V_g dependence; this spurious voltage does not significantly change the shape of the thermovoltage characteristics, and can be safely subtracted. Figures 1(c) and 1(d) show G and V_{th} characteristics measured at $T_L=4.2$ K for samples I and III, with the linear background subtracted from $V_{th}(V_g)$. Theoretically the thermopower S is related to the derivative of the conductance G via the Cutler-Mott relation,[8]

$$S = \frac{-V_{th}}{T_e - T_L} = -\frac{\pi^2 k_B^2}{3e}(T_e + T_L)\frac{1}{G}\frac{\partial G}{\partial \mu}, \quad (1)$$

where μ is the chemical potential. As successive 1D subbands are opened up for transmission, the conductance rises in steps of $2e^2/h$. Equation (1) predicts that each step is accompanied by a peak in the thermovoltage $V_{th}(V_g)$; the dotted vertical lines in Figs. 1(c) and 1(d) show this alignment for samples I and III, respectively.

To illustrate how the linear contribution to $V_{th}(V_g)$ is subtracted, Fig. 2(a) shows the raw thermovoltage of sample I at 4.2 K for different heating currents I_H from 0.5 to 5 μA, with the data shifted vertically for clarity. The dashed line shows the linear contribution at I_H=5 μA, which is much smaller than the overall signal, and does not change the shape or position of the peaks. Figure 2(a) shows how the heights V_{pk}^i of the thermovoltage peaks vary with heating current I_H, and the Fig. 2(a) inset shows the height of the first thermovoltage peak V_{pk}^1 plotted as a function of I_H^2, the square of the heating current. For heating currents I_H up to 2.5 μA, the peak height V_{pk}^1 scales with the heating power, $I_H^2 R_H$, where R_H=390 Ω is the resistance of the heating channel. At T_L=4.2 K a heating current of I_H=1 μA heats the electrons by ΔT=71 mK. The power dissipated per electron is $P = I_H^2 R_H / n_e A_H$, where A_H is the area of the heating channel. In our samples A_H=155 μm^2, which is the effective area of the Hall bar through which I_H is injected [see Fig. 1(a)]. If the electrons are heated to a temperature T_e they exchange energy with phonons at temperature T_L, and the net power transfer from the electrons to the lattice is given by

$$P = \dot{Q}(T_e) - \dot{Q}(T_L). \quad (2)$$

The energy-loss rate $\dot{Q}(T)$ can be measured experimentally[4] and compared to theoretical predictions. Other sources of energy loss, for example, through the Ohmic contacts are very small, and can be detected[4] only at low temperatures.

Within the saddle-point model[9] the thermovoltage peaks have a height[10]

$$V_{pk}^i = \frac{\pi^3 k_B^2}{24 e \hbar \omega_x}\frac{(T_e^2 - T_L^2)}{(i + 1/2)}, \quad (3)$$

where i is the subband index and $\hbar\omega_x$ is the characteristic energy width of the risers between the conductance steps. Assuming a saddle-point potential for the constriction we fit the conductance characteristics $G(V_g)$ to obtain ω_y/ω_x (for example, the ratio is 2.76 for sample I), and then ω_x is determined knowing the 1D subband spacing $\hbar\omega_y$, which is obtained from source-drain voltage measurements. Inputting this information into Eq. (3), the electron temperature T_e can be determined from the height of the first thermovoltage peak V_{pk}^1.

Before presenting T_e measurements we first demonstrate the validity of Eqs. (1) and (3). If thermovoltage traces $V_{th}(V_g)$ measured at different I_H are normalized by the magnitude of one of the thermovoltage peaks, the equations predict a collapse of the data onto a single trace when the thermal broadening is much less than the subband spacing. Figure 2(b) shows $V_{th}(V_g)$ traces for sample I normalized by

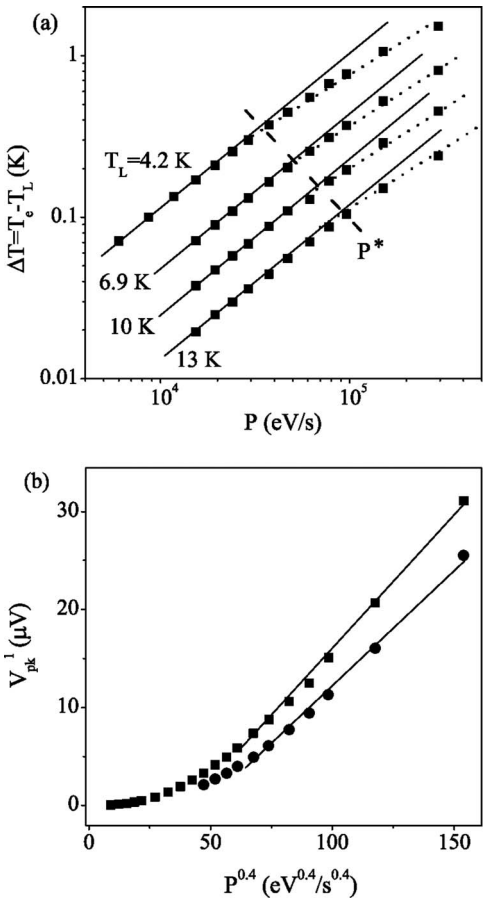

FIG. 3. (a) The difference between the electron and lattice temperatures $\Delta T = T_e - T_L$, as a function of heating power P, for four different lattice temperatures. P^* is the power at which there is a deviation from linear behavior. (b) Sample I: the height of the first thermovoltage peak V_{pk}^1 as a function of $P^{0.4}$ at T_L=4.2 (■) and 6.9 K (•).

the magnitude of the first (i=1) thermovoltage peak V_{pk}^1 for heating currents I_H=0.5–6 μA. All the traces collapse onto a single curve, in agreement with previous measurements[4] of split-gate devices. The dashed trace shows the thermal broadening at I_H=7 μA. The right inset of Fig. 2(b) shows plots for sample I taken with I_H=1.6–5 μA for lattice temperatures T_L=4.2–13 K; again all the data collapse onto a single curve. The left inset of Fig. 2(b) shows the normalized peak heights V_{pk}^i/V_{pk}^3 for all three samples lying on the curve $3.5/(i+1/2)$, which is derived from Eq. (3).

Having established the conditions for linear thermopower measurements, we investigate the electron temperature T_e of the 2DEG for different heating powers P and lattice temperatures. Figure 3(a) shows a log-log plot of $\Delta T = T_e - T_L$ versus P for four different T_L. At low heating powers ΔT scales linearly with P, as shown by the solid straight lines and in agreement with the results presented in the Fig. 2(a) inset. At higher heating powers, $\Delta T(P)$ becomes sublinear when the conditions $\Delta T \ll T_L$ and $V_{pk}^1 \propto \Delta T$ are no longer satisfied. The power at which this deviation occurs is labeled as P^* in Fig. 3(a); P^* increases with increasing T_L, which is the expected behavior due to the increase in the number of scattering phonons with temperature.

Previous measurements[4] show that the thermovoltage peak heights V_{pk}^1 taken at different T_L converge at high power to follow the form $V_{pk}^1 \sim P^{0.4}$. This occurs for $T_e \gg T_L$, when the energy-loss rate in Eq. (2) becomes $P \approx \dot{Q}(T_e)$ and is independent of T_L. In this limit Eq. (3) has the form $V_{pk}^1 \sim T_e^2$, and $P^{0.4}$ behavior will occur if $\dot{Q} \propto T_e^5$. This T^5 behavior was attributed[4] to acoustic phonon scattering in the Grüneisen-Bloch regime, with coupling via a screened piezoelectric potential.[11] These previous measurements[4] were performed at $T_L \leq 1.5$ and $T_e \leq 3$ K, with heating powers $P \leq 10^4$ eV/s, and the transition to $P^{0.4}$ behavior occurred at a power which is an order of magnitude smaller than the convergence point.

At higher lattice temperatures more heating power is needed to reach the limit $T_e \gg T_L$ and the associated convergence of the $V_{pk}^1(P)$ traces, a regime we have not investigated in detail. We find, however, that at the two lowest lattice temperatures $T_L = 4.2$ and 6.9 K, there is a crossover with increasing P from linear to $V_{pk}^1(P) \sim P^{0.4}$ behavior. This is shown in Fig. 3(b) and is in agreement with previous results[4] obtained for $T_L \leq 1.5$ K.

To investigate the scattering mechanisms in the 2DEG we present the dissipated power P measured as a function of the electron temperature T_e. Figure 4(a) shows the results at $T_L = 4.2$ K as a log-linear plot, and a fit to the data was obtained putting an energy-loss rate $\dot{Q} \sim T^5$ into Eq. (2) to give $P = A(T_e^5 - T_L^5)$, where the fitting parameter was found to be $A = 57 \pm 2$ eV/s K^5. The coefficient of the T^5 behavior is close to that obtained[4] ($A = 61$ eV/s K^5) in split-gate devices for $T_e < 3$ K, which was attributed to a screened PZ mechanism. According to the conventional theory of phonon scattering, T^5 behavior can also be obtained with an *unscreened* deformation potential coupling; the theoretical value[11,12] for the constant of proportionality is $A_{th}^{DP} = 76$ eV/s K^5, which is close to that measured at 4.2 K. The potentials for acoustic phonon scattering are screened when both T_L and T_e are much less than T_s, where $T_s = \hbar s_t / r_s k_B$, $r_s = \sqrt{\pi a_B / 4 k_F}$ is the Thomas-Fermi screening length, and a_B is the effective Bohr radius. For our devices $T_s \approx 4$ K, and as all the data presented here were measured at temperatures $T \geq 4.2$ K, the screening conditions are not satisfied and the unscreened behavior is expected to dominate. Calculations of the unscreened PZ contribution to the acoustic phonon scattering give $\dot{Q}_{PZ} = 485T^3$ eV/s; this is shown by the gray line in Fig. 4(a) and has the incorrect functional form and magnitude compared to the measurements. Moreover unscreened PZ behavior at 4.2 K is approximately three times smaller than the DP term, $\dot{Q}_{DP} = 76T^5$ eV/s.

Calculations[12] using formulas derived by Jasiukiewicz and Karpus[11] show that for screened potentials the T^7 term due to DP scattering dominates over the PZ term for $T_L > 2.5$ K; this is seen from the comparison of $\dot{Q}_{PZ} = 325T^5$ eV/s and $\dot{Q}_{DP} = 50T^7$ eV/s. We have tried fitting the data at 4.2 K to a T^7 dependence, as shown by the dotted line in Fig. 4(a); however, not only is the fit significantly worse than that of T^5, but also the obtained dependence, $\dot{Q} = 1.6T^7$ eV/s, is much smaller than theoretical expectations $\dot{Q}_{DP}$.

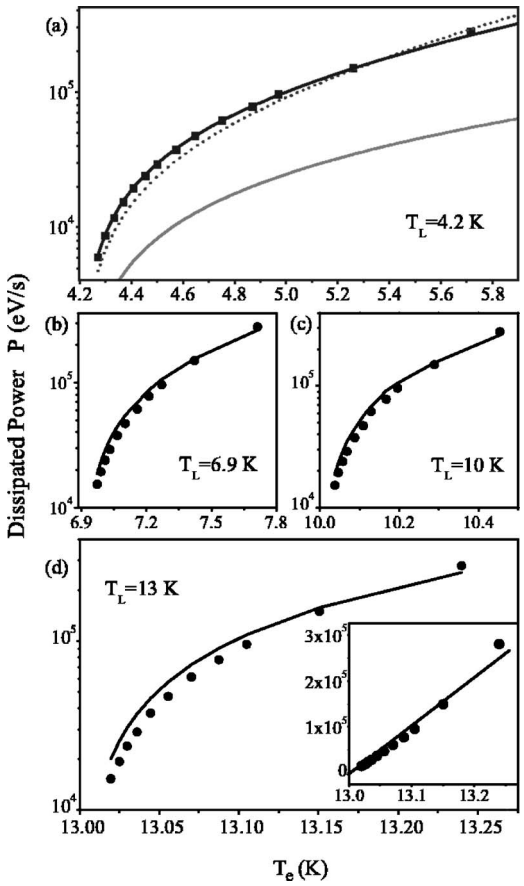

FIG. 4. Dissipated power P as a function of electron temperature T_e at T_L= (a) 4.2, (b) 6.9, (c) 10, and (d) 13 K. The solid lines are best fits to $P = A(T_e^5 - T_L^5)$ with the values of A given in Table I. In (a) the dotted line is the best fit using $\dot{Q} \sim T^7$, and the gray solid line is the expected behavior $P = 485(T_e^3 - T_L^3)$ eV/s for the unscreened PZ potential. The inset to (d) shows a linear-linear plot.

In summary, the best description of the data at $T_L = 4.2$ K is obtained by a T^5 fit with a coefficient $A = 57$ eV/s K^5, close to the theoretical value $A_{th}^{DP} = 76$ eV/s K^5, suggesting the dominance of the unscreened deformation potential coupling in the phonon scattering. Considering previous experimental results,[4] there is probably a transition between screened PZ and unscreened DP coupling at around $T_s \approx 4$ K. As well as having the same functional form for the energy loss, $\dot{Q} \sim T^5$, the experimental coefficients for both regimes $T < T_s$ and $T \gtrsim T_s$ are also very similar.

Figures 4(b)–4(d) show the dissipated power P for T_L above liquid helium temperatures. The fits to $P = A(T_e^5 - T_L^4)$ remain good with the values of A listed in Table I; the most noticeable trend is the sharp decrease of A with lattice temperature, such that at 13 K it is nearly an order of magnitude smaller than at $T_L = 4.2$ K. At the higher lattice temperatures, $T_L \geq 6.9$ K, there is a proportionally smaller amount of heating ΔT for a given current I_H, and because the power loss is dominated by the linear term (for example, see inset to Fig. 4(d)), $P = A(T_e^n - T_L^n) \approx An(T_e - T_L)T_L^{n-1}$, it is not possible to distinguish T^5 from T^7 behavior. However, similar to the T^5 fits, the coefficient for the T^7 fits is rapidly decreasing from

TABLE I. The fitting parameters at four different lattice temperatures. The coefficient A is obtained from fits of $P=A(T_e^5-T_L^5)$ to the data in Figs. 4(a)–4(d); A^* and T_0 are obtained from fits of Eq. (4) to the data in Figs. 5(a)–5(d).

T_L (K)	A (eV/s K^5)	A^* (eV/s K^5)	T_0 (K)
4.2	57±2	62±3	10±0.5
6.9	23±3	52±8	8.4±0.5
10	10.4±1	59±4	9.0±0.5
13	7.2±1	56±4	10.3±0.5

its $T_L=4.2$ K value (1.6 eV/s K^7) as T_L is increased, becoming much smaller than theoretical expectations (50 eV/s K^7).

It should be stressed that there are no theoretical expressions for $\dot{Q}(T)$ in the intermediate temperature regime when $T\sim T_{GB}$. For our samples $T_{GB}\approx 8.6$ K, which is roughly in the middle of the measured temperature range. Previously the temperature dependence of the mobility due to acoustic phonon scattering has been modeled[13] in this intermediate regime with a phenomenological formula, and using a similar approach we put forward the following expression for the energy-loss rate:

$$\dot{Q}=\frac{A^*T^5}{1+(T/T_0)^4}. \tag{4}$$

Equation (4) provides the correct limiting behavior in the low- ($\dot{Q}\propto T_e^5$) and high-temperature ($\dot{Q}\propto T_e$) regimes. At low temperatures A^* is a coefficient similar to A, and T_0 is a temperature that characterizes the transition to the equipartition regime, which is expected[13] to be of the order of T_{GB}.

The energy transfer function $\dot{Q}(T_e)$ is plotted in Fig. 5 together with fits to Eq. (4), and using this interpolation formula, rather than pure T^5 behavior, the quality of the fits is better than in Fig. 4. The fitted values for A^* and T_0 given in Table I are practically independent of the lattice temperature, and they are close to the theoretical values of A_{th}^{DP} and T_{BG}, respectively. In Fig. 5(e) the data measured at different T_L from 4.2 to 13 K are plotted together with a single fit using the average values, $A^*=59$ eV/s K^5 and $T_0=10$ K. From the favorable fit to the results we conclude that the intermediate regime is realized at 10 K.

The electron power dissipation has already been investigated using the temperature dependence of the mobility[6,14,15] and the Shubnikov–de Haas (SdH) oscillations[16,17] as a thermometer. The former method has limited applicability due to a contribution from impurity scattering to the temperature dependence of the mobility; it has been shown[18,19] that interference effects are possible between electron-impurity and electron-phonon scattering, making it difficult to separate the two. In a direct comparison of the SdH oscillation method with thermopower thermometry, it was found[4] that the temperature dependence of the energy-loss rates are strongly perturbed by a weak magnetic field, changing the temperature behavior from $\dot{Q}\propto T^5$ to T^3. This leads to an underestimate of the power dissipated per electron using the SdH method.

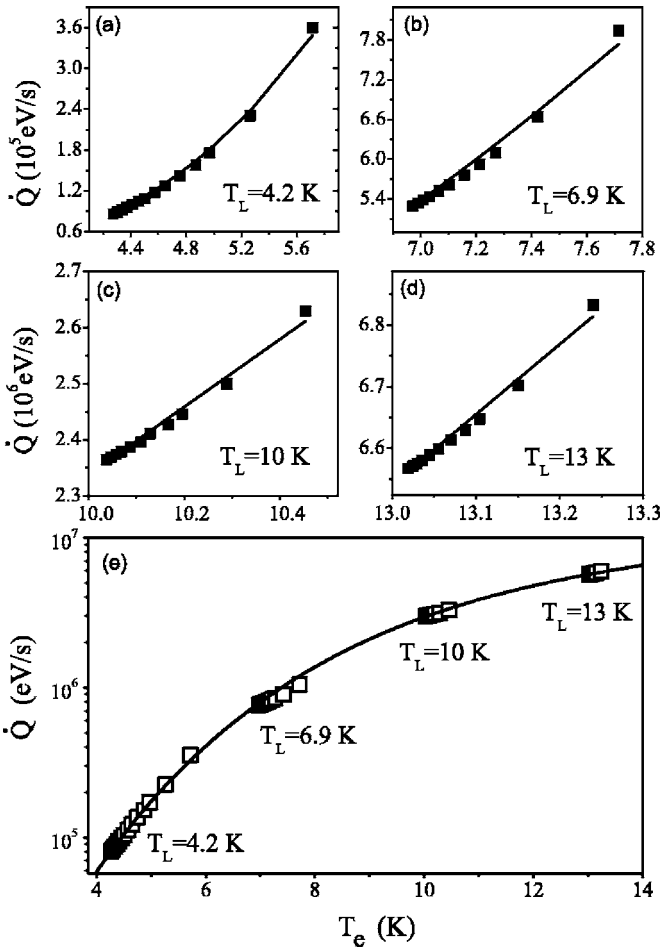

FIG. 5. Power transfer per electron, $\dot{Q}$, versus the electron temperature T_e for lattice temperatures (a) $T_L=4.2$, (b) 6.9, (c) 10, and (d) 13 K. The solid lines are fits to Eq. (4) using the parameters A^* and T_0 listed in Table I. (e) All the data in (a)–(d) plotted together with a solid line fit using $A^*=59$ eV/s K^5 and $T_0=10$ K.

Moreover, when thermometry based on mobility and SdH is applied to GaAs/Al$_x$Ga$_{1-x}$As heterostructures an anomalously large deformation potential constant ($E_1\approx 11-13$ eV) is obtained,[6,14–16] in strong disagreement with the conventional value ($E_1=7$ eV), and which led to a debate about its possible enhancement (see, for example, Ref. 20). In contrast to the above two methods, electron thermometry from the thermopower bypasses both the influence of impurity scattering and the necessity for a magnetic field. We find that all of our results can be self-consistently described by a formulation using the conventional value $E_1=7$ eV. We should, however, stress that due to a lack of a theoretical description in the intermediate regime, we have had to propose our own interpolation formula [Eq. (4)]. To fully substantiate our conclusions regarding the transition into the equipartition regime, further experiments and/or theoretical developments will be needed.

IV. CONCLUSIONS

In summary, we have investigated the thermopower of 1D constrictions in GaAs/Al$_x$Ga$_{1-x}$As heterostructures, extend-

ing the temperature range of energy-loss studies of a 2DEG at zero magnetic field. The measurements use wet-etched devices with hard-wall potentials and large 1D subband spacings, providing a simple and reliable means for thermovoltage measurements $V_{th}(V_g)$ at high lattice temperatures. By varying the heating current I_H the temperature T_e of electrons in the channel adjacent to the constriction has been measured up to 13 K, and the power dissipation per electron P has been calculated.

At $T_L=4.2$ K our measurements show that the energy-loss rate is $\dot{Q}\sim T^5$; although this behavior is consistent with previous measurements[4] at lower temperatures, we believe that these results obtained at temperatures close to T_s are described by an unscreened deformation potential rather than a screened piezoelectric potential. For lattice temperatures $T_L > 4.2$ K the coefficient (A) of the T^5 behavior is reduced dramatically. The dissipated power cannot be described by T^5 dependence alone, due to a crossover to the intermediate regime where T_L and T_e are of the order of T_{GB}. It is found that the experimental results in the range $T_L=4.2-13$ K can be described by a phenomenological equation that contains only temperature independent coefficients, and has the correct limiting behavior in both the low-temperature and equipartition regimes.

*Present address: Department of Micro and Nanotechnology, Technical University of Denmark (DTU), DK-2800 Kongens Lyngby, Denmark.

[1] B. J. van Wees, H. van Houten, C. W. J. Beenakker, J. G. Williamson, L. P. Kouwenhoven, D. van der Marel, and C. T. Foxon, Phys. Rev. Lett. **60**, 848 (1988).
[2] D. A. Wharam, T. J. Thornton, R. Newbury, M. Pepper, H. Ahmed, J. E. F. Frost, D. G. Hasko, D. C. Peacock, D. A. Ritchie, and G. A. C. Jones, J. Phys. C **21**, 209 (1988).
[3] L. W. Molenkamp, H. van Houten, C. W. J. Beenakker, R. Eppenga, and C. T. Foxon, Phys. Rev. Lett. **65**, 1052 (1990).
[4] N. J. Appleyard, J. T. Nicholls, M. Y. Simmons, W. R. Tribe, and M. Pepper, Phys. Rev. Lett. **81**, 3491 (1998).
[5] O. Chiatti, J. T. Nicholls, Y. Y. Proskuryakov, N. Lumpkin, I. Farrer, and D. A. Ritchie, Phys. Rev. Lett. **97**, 056601 (2006).
[6] H. L. Stormer, L. N. Pfeiffer, K. W. Baldwin, and K. W. West, Phys. Rev. B **41**, 1278 (1990).
[7] A. Kristensen, H. Bruus, A. E. Hansen, J. B. Jensen, P. E. Lindelof, C. J. Marckmann, J. Nygard, C. B. Sorensen, F. Beuscher, A. Forchel, and M. Michel, Phys. Rev. B **62**, 10950 (2000).
[8] M. Cutler and N. F. Mott, Phys. Rev. **181**, 1336 (1969).
[9] H. A. Fertig and B. I. Halperin, Phys. Rev. B **36**, 7969 (1987).
[10] C. R. Proetto, Phys. Rev. B **44**, 9096 (1991).
[11] C. Jasiukiewicz and V. Karpus, Semicond. Sci. Technol. **11**, 1777 (1996).
[12] For our calculations we take the deformation potential constant for GaAs to be $E_1=7$ eV.
[13] V. Karpus, Semicond. Sci. Technol. **5**, 691 (1990).
[14] E. E. Mendez, P. J. Price, and M. Heiblum, Appl. Phys. Lett. **45**, 294 (1984).
[15] B. J. F. Lin, D. C. Tsui, and G. Weimann, Solid State Commun. **56**, 287 (1985).
[16] K. Hirakawa and H. Sakaki, Appl. Phys. Lett. **49**, 889 (1986).
[17] Y. Ma, R. Fletcher, E. Zaremba, M. D'Iorio, C. T. Foxon, and J. J. Harris, Phys. Rev. B **43**, 9033 (1991).
[18] A. Sergeev and V. Mitin, Phys. Rev. B **61**, 6041 (2000); A. Sergeev, M. Y. Reizer, and V. Mitin, *ibid.* **69**, 075310 (2004).
[19] M. Y. Reiser and A. V. Sergeev, Sov. Phys. JETP **65**, 1291 (1987).
[20] W. Walukiewicz, H. E. Ruda, J. Lagowski, and H. C. Gatos, Phys. Rev. B **32**, 2645 (1985).